Estuarine, Coastal and Shelf Science 246 (2020) 107028

Contents lists available at ScienceDirect

Estuarine, Coastal and Shelf Science

journal homepage: http://www.elsevier.com/locate/ecss

New validation method for hydrodynamic fjord models applied in the Hardangerfjord, Norway

Stig B. Dalsøren *, Jon Albretsen, Lars Asplin

Institute of Marine Research, PO Box 1870 Nordnes, 5817, Bergen, Norway

ARTICLE INFO

Keywords:
Hydrodynamic model
Current measurements
Validation method
Fjords
Hardangerfjord
Norway

ABSTRACT

We introduce a new intuitive evaluation method for comparison of fjord model results and current measurements. The approach is tested using high resolution model simulations and measurements in the Hardangerfjord, a large fjord system in Norway with huge aquaculture production. The method is easy to interpret, clearly distinguishes periods with good and poor model performance, and relate them to physical driving forces. This makes it possible to identify potential shortcomings in the models' representation of physical processes.

The applied model mostly performs well in the Hardangerfjord. Good performance often coincides with strong local fjord forcing (i.e. strong winds in the fjord). In periods with poor model performance, internal waves induced by pressure perturbations on the coastal shelf tend to propagate erroneously into the fjord. Stratification biases in coastal waters, connected to the applied model boundary conditions, seems to be an important cause.

Demonstrated flexibility of time frame and performance criteria suggests applicability of the validation method for a wide set of geophysical variables in various physical environments.

1. Introduction

Currently, mariculture is practiced in more than 100 countries (Oyinlola et al., 2018). Open facilities are often used, allowing for free water exchange with the surrounding marine environment. Growth and survival of farmed organisms thereby depend on the physical and chemical properties of the entering water. In turn, water properties of the surroundings are affected by the farms. Current, temperature, and salinity output from hydrodynamic model systems are used as input for Lagrangian particle-drift models predicting salmon lice infestation pressure for such environments (Adams et al., 2015; Asplin et al., 2014; Foreman et al., 2015; Gillibrand and Willis, 2007; Johnsen et al., 2016; Kragesteen et al., 2018; Myksvoll et al., 2018; Rogers et al., 2013; Salama and Rabe, 2013; Salama et al., 2018; Sandvik et al., 2016a, 2020). For these and other studies (e.g. dispersion of pollution, pathogens, harmful algal blooms), it is important to reveal: How well hydrodynamic models reproduce reality, underlying causes for correspondence and mismatch, and ways to improve the models. Information on the model accuracy is also often asked for by the industry, authorities, and public.

Numerous accuracy measure indexes on how model results reproduce measurement data exist (Armstrong and Collopy, 1992; Chen et al., 2017; Duveiller et al., 2016; Shcherbakov et al., 2013). However, many of the traditional used indexes such as the Pearson correlation coefficient (r), coefficient of determination (R^2) and root mean square error (RMSE) suffer from one or more shortcomings such as poor resistance to outliers, asymmetry, and scale dependencies (Armstrong, 2001; Chen et al., 2017; Duveiller et al., 2016; Shcherbakov et al., 2013). Scatter-, histogram-, quantile-quantile plots and Taylor diagrams are much used graphical presentation forms, the last visualizing concurrently various metrics that contain complementary information. However, their interpretation is not straightforward for the broad user group referred to in the last paragraph and may be hampered by shortcomings in the metrics forming their basis. These are major reasons why we suggest a new evaluation method summarizing agreement by a single index that fulfill criteria for good accuracy measures (Adams et al., 2015; Armstrong and Collopy, 1992; Clements and Hendry, 1993; Fildes, 1992). We apply the accuracy measure index λ suggested by Duveiller et al. (2016), presented in more detail in the methods section. We also introduce a graphical visualization approach (Methods and Results section) categorizing model performance. Its presentation form is easy to interpret and intuitive, thereby understandable for a broad interest group consisting of scientist, spatial planners, decision makers etc. A critical value of λ, λ_{crit}, is chosen and above that value the model performance is characterized as good. Since λ is easy to compute,

* Corresponding author.
E-mail address: stig.dalsoeren@hi.no (S.B. Dalsøren).

https://doi.org/10.1016/j.ecss.2020.107028
Received 13 June 2020; Received in revised form 16 September 2020; Accepted 23 September 2020
Available online 29 September 2020

a-dimensional, scale-independent, and bounded, computation can be made at many depth levels and locations using a single critical value (λ_{crit}) which is not the case for several other indexes not fulfilling these criteria. The use of the method is demonstrated for the Hardangerfjord in Norway.

Norway is one of the world's largest producers of Atlantic salmon. The Norwegian government has implemented a management system for aquaculture using traffic lights (green–yellow–red) to control the growth in an environmentally sustainable way (Myksvoll et al., 2018). There are several risk factors that may hamper a sustainable aquaculture and increase in salmon farming in Norway (Grefsrud et al., 2019; Taranger et al., 2014; Torrissen et al., 2013). The effect of parasitic salmon lice, released from salmon farms, on the mortality of wild salmonid fish is currently used as indicator for the traffic light system. Output from the hydrodynamic model applied in this study is used as input for a particle-drift model predicting infestation pressure providing information for the traffic light assessment (Myksvoll et al., 2018; Sandvik et al., 2020). It is therefore important to document model performance by a reliable and intuitive method. For the Hardangerfjord, this is particularly important as the production area which includes the fjord in February 2020 was given a yellow light. This means that the production is not allowed to increase until the next vulnerability assessment is made after two years (autumn 2021). The fjord has one of the world's densest concentrations of farmed salmonid fish with a yearly production of about 80,000 tons (Sandvik et al., 2020).

The 183 km long Hardangerfjord situated on the Norwegian west coast (Fig. 1), is Norway's second longest fjord. The main fjord has four basins separated by shallower sills (Fig. 1). The largest basin depth is

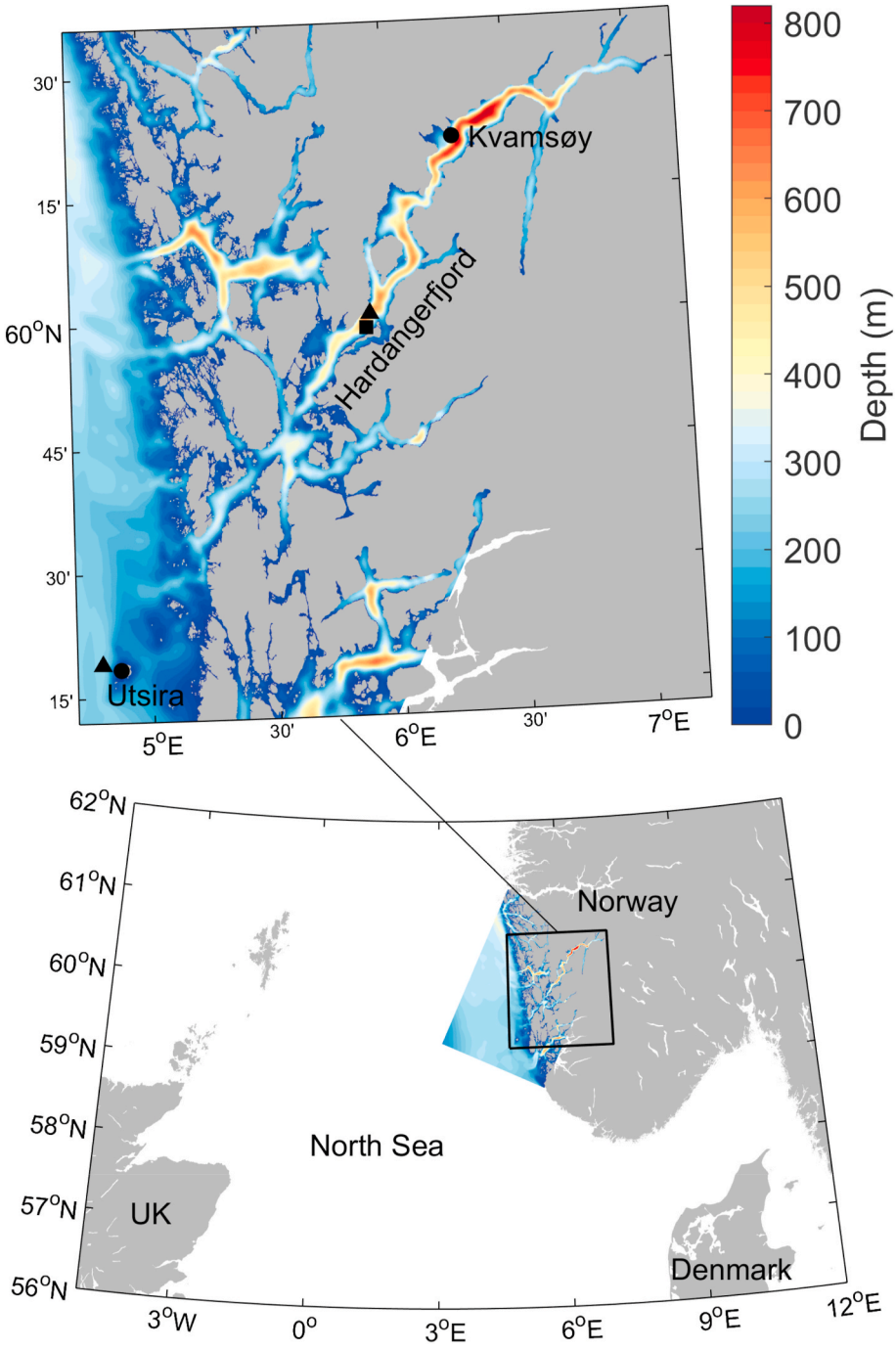

Fig. 1. Upper panel: Bathymetry in and near the Hardangerfjord in the high resolution (160 m × 160 m) hydrodynamic model presented here and locations (black symbols) of measurement sites: Square: Acoustic Doppler Current Profiler (ADCP) located mid-fjord. Triangles: CTD (Conductivity, Temperature and Depth) locations where profiles of salinity and temperature were measured (an offshore site, outer Utsira, and a mid-fjord site). Circles: Wind measurements from the Utsira (offshore) and Kvamsøy (inner/mid-fjord) islands. Lower panel: Geographical location of the model domain (shown by its bathymetry) adjacent to the northern North Sea.

820 m while the shallowest sill is at about 180 m depth. The width of the main fjord ranges from about 2 to 7 km. At the inner part, the main fjord branches into several narrow side fjords. There are several large rivers in the region, and in the side fjords the surface water is usually brackish. The yearly average flux from all rivers discharging to the fjord is typically in the range 500–800 m^3/s but inter-annual, seasonal, and day to day variation are large (Sjøtun et al., 2015). On seasonal basis, fluxes often have maximums in late spring due to snow melt in the surrounding mountains and in fall-early winter due to heavy precipitation (Sjøtun et al., 2015).

The main fjord connects to the ocean (the northern North Sea) through one main fjord mouth and three narrower channels to the north (Fig. 1). On the coastal shelf, outside the fjord mouth, depths are 40–200 m over much of the area except for some deeper troughs. At the coast and in the outer fjord the dominant wind direction is approximately north-south (typically 60–65% of the time (Mayer et al., 2020)). In the mid-inner main fjord, the wind tends to be steered by channeling action of steep mountain sides and mainly follow the up- and downwind directions of the fjord.

In the Hardangerfjord, currents have the potential to transport salmon lice over long distances (up to 100 km) during their pelagic phase (Asplin et al., 2014) and their vertical position depends on physical conditions like temperature and salinity (Crosbie et al., 2019, 2020; Johnsen et al., 2014; Samsing et al., 2016). Better understanding of the circulation and hydrography of the upper water masses in the fjord, where lice and migrating salmon often reside (Crosbie et al., 2019, 2020; Davidsen et al., 2008; Johnsen et al., 2014; Samsing et al., 2016; Sandvik et al., 2020), is a prerequisite to take the right action to evaluate the infestation pressure.

The circulation in the Hardangerfjord shares many of the features reported for other mid-latitude fjords with similar geophysical characteristics (Farmer and Freeland, 1983; Inall and Gillibrand, 2010; Inall et al., 2015; Stigebrandt, 2012; Wan et al., 2017). The major driving factors for the circulation in these fjords are freshwater input, tides, local winds, and external fluctuations in stratification on the coastal shelf. Freshwater input drives exchange via shear entrainment at or near the surface. The supply of freshwater to the fjord stratifies the water column. A shallow quite well mixed layer with light outflowing fjord water develops in the inner fjord overlaying denser water below, and a density gradient (the pycnocline) separates these water masses. The upper layer of fjord water becomes more saline on its way toward the fjord mouth due to mixing and entrainment. Wind induces momentum stress on the water surface and in strong events it may be decisive for current strength and direction (Castillo et al., 2017; Svendsen and Thompson, 1978), and vigorous mixing may move the pycnocline downward. Tides affect the whole water column and may drive both barotropic (tidal pumping), and baroclinic exchange (diapycnal mixing).

Stratification fluctuations external to the fjord mouth affect the fjord circulation, especially intermediary exchange. Density variations outside the fjord set up a pressure gradient force between the fjord and shelf driving baroclinic flows within the fjord (Arneborg et al., 2004; Asplin et al., 1999; Jackson et al., 2018; Klinck et al., 1981; Stigebrandt, 1990; Sundfjord, 2010). These low frequency density fluctuations in coastal water is the dominant exchange mechanism with the shelf for a typical fjord on the Norwegian west coast (Stigebrandt, 1990). The characteristics of the associated fjord flows depend on the fjord width and length (i.e. internal Rossby radius of deformation of the fjord, 3D dynamics are integral for radius >0.5), forcing period and amplitude, and the initial vertical stratification on the coastal shelf (Jackson et al., 2018; Sundfjord, 2010).

One mechanism for coastal density variations is wind-induced coastal convergence or divergence of the surface Ekman layer. In the Northern Hemisphere, the net wind-driven transport of water is to the right of the wind direction. Along the western coast of Norway, northward wind thus results in onshore water transport near the surface. The widths of the associated coastal currents are typically comparable to the internal Rossby radius of deformation. Near the coastal wall there will then be a rise of the sea surface, downwelling below, and deepening of the pycnocline. Where the coastline is broken by a fjord, these movements set up a horizontal pressure gradient at the fjord mouth and internal waves propagate into the fjords. The propagating waves sets up a temporary current field driving exchange between the coast and fjord and locally inside the fjord. The induced current signal in the fjord will be directed into the fjord above the pycnocline and out of the fjord below. For southward wind, there will be offshore transport of coastal water near the surface, upwelling near the coast and a rise of the pycnocline. This results in outward flow above the pycnocline and inward below. We adopt nomenclature from Asplin et al. (1999) and in the following sections we denote this type of circulation as "nonlocal wind driven coast-fjord advection".

Advection of water-masses with different properties can also result in density fluctuations on the coastal shelf and induce flow into or out of the fjord. The Norwegian Coastal Current (NCC) is an important dynamic feature along the coast with high spatial and temporal variability that interacts with the nonlocal wind driven coast-fjord advection (Sætre, 2007). The cold and fresh NCC is wedged between the warm and saline Norwegian Atlantic Current and the coast. In the summer, it is wide and shallow, while in the winter it turns narrow and deep. Typical current speeds in the NCC are about 0.2–0.5 m/s, with maximum speeds exceeding 1 m/s.

Particularly for the Hardangerfjord, Sundfjord (2010) and partly Asplin et al. (2014) discuss the contribution from nonlocal wind driven coast-fjord advection. They show that the associated internal waves and current signals only establish far into the fjord if rather strong alongshore winds sustain over several days. Other studies (Asplin et al., 2014; Azad et al., 2019; Husa et al., 2014; Johnsen et al., 2014; Sandvik et al., 2020; Skogen et al., 2009), focusing on marine biology and food security, briefly discuss the general circulation of the fjord system or parts of the main fjord.

2. Methods

2.1. Hydrodynamic model

In this study, we apply the open-source Regional Ocean Modeling System (ROMS) (Haidvogel et al., 2008; Shchepetkin and McWilliams, 2005) (see also http://myroms.org) which is a state-of-the-art, three--dimensional, free-surface, hydrostatic, primitive equation ocean model that uses generalized terrain-following s-coordinates in the vertical. The model grid used in the present work covers the Hardangerfjord and surrounding areas (Fig. 1) with 160 m × 160 m resolution in the horizontal and applies 35 vertical levels. This model version, named NorFjords-160, has been applied in several recent studies (Filbee-Dexter et al., 2020; Simonsen et al., 2019; Skarðhamar et al., 2018).

The bathymetry data was downloaded from the online data source, http://www.norgedigitalt.no, established by the Norwegian Mapping Authority, the Hydrographic service. Tides from TPXO7.2 global tidal analysis were included (Egbert and Erofeeva, 2002). Daily river flow rates from 170 rivers were included in the NorFjords-160 simulations and based on estimates from the Norwegian Water Resources and Energy Directorate (NVE) through their updated data series from all catchment areas in Norway (http://nve.no). These data series use measured water flows to estimate the total runoff along the coastline within each catchment area. As there are several main rivers within each catchment area, we separated the flow according to each river's upstream area. Atmospheric forcing was provided from AROME MetCoOp (Meteorological Co-operation on Operational Numerical Weather Prediction) 2.5 km, the main forecasting system at the Norwegian Meteorological Institute (Müller et al., 2017).

Initial hydrodynamic fields were obtained from parts of a 25-year hindcast archive from the 800 m × 800 m resolution model NorKyst-800 covering the Norwegian coast. Details and results from this model

archive are presented in Asplin et al. (2020). Hydrodynamic forcing along the NorFjords-160 open boundaries was taken as hourly fields from this archive. The Chapman boundary condition (Chapman, 1985) was used for the free-surface boundary condition and the Flather boundary condition (Flather, 1976) was applied for the barotropic velocity. The applied method (Marchesiello et al., 2001) provide radiation conditions on outflow and nudging to a known exterior value on inflow for 3D momentum and tracers (one-way nesting, see Asplin et al. (2020) for details). When compared with temperature, salinity, and current measurements, NorKyst-800 mostly shows good correspondence (Asplin et al., 2020). The focus was then on long time scales (monthly, seasonal and yearly averages) using traditional graphical presentation forms and accuracy measure indexes. The evaluation method introduced in this study categorizing model performance over defined time frames of a few days has yet not been applied but will be implemented in future studies. NorKyst-800 is also run operationally at the Norwegian Meteorological Institute (http://thredds.met.no) providing daily forecasts.

The Norfjords-160 simulations were performed from March throughout August 2016 and March 2017 throughout December 2018 covering periods with rather frequent current and hydrographic measurements in the Hardangerfjord. The model was run with an internal time-step of 6 s, writing output data for temperature, salinity, currents, etc. every hour. In this work, we focus on the subtidal circulation and in the presented current results the model output and measurement data were detided using the t-tide toolbox for Matlab (Pawlowicz et al., 2002), then a 4th order Butterworth lowpass filter with a 24 h cutoff period was applied. In the comparison with measurements the closest model grid box is used. Representativeness is further touched upon in the Discussion section.

2.2. Measurements

CTD measurements of temperature and salinity have been performed approximately bi-monthly in the main branch of the Hardangerfjord and occasionally in some side fjords since 2004. In this study, we apply measurements from the CTD site closest to the ADCP site (Fig. 1). The instrument used is a SAIV SD204 mini CTD (http://www.saivas.no). The technical specifications for the SD204 are: Sampling interval 1 s, resolution of temperature sensor 0.0018 °C, accuracy of temperature sensor ±0.018 °C, response time of temperature sensor 0.2 s, resolution of pressure sensor 0.01 dbar, accuracy of pressure sensor ±0.01% FS (sampling frequency), response time 0.1 s. The Institute of Marine Research also has eight coastal monitoring stations for hydrographic measurements along the coast (Albretsen et al., 2011), (http://www.imr.no/forskning/forskningsdata/stasjoner). At these stations, profiles are collected approximately twice a month by CTD sampling, also using the SAIV SD204. The outer and inner Utsira stations are in vicinity of the mouth of the Hardangerfjord. Profiles from outer Utsira (location shown in Fig. 1) are used as a proxy for the coastal stratification since it is far enough from the fjord mouth to be relatively unaffected by fjord inflow/outflow.

Wind measurements were retrieved from the Norwegian Meteorological Institute weather and climate database eKlima (http://eklima.met.no). We compare modeled and measured coastal wind at the Utsira island. The fjord wind is evaluated at the Kvamsøy island, which is the measurement site situated closest to the ADCP site (see map in Fig. 1). The measurement data is available as hourly means and the sampling height is 10 m. Both stations are part of the official network of the Norwegian Meteorological institute and measurements flagged "very uncertain" by their quality control were discarded.

The current mooring was located approximately midway in the main fjord (square Fig. 1) about 45 km from the fjord mouth. Moored Acoustic Doppler Current Profilers (ADCP) were used, situated at depths from 12 to 32 m, measuring upwards and downwards using the Doppler shift to estimate currents. Instruments of type Nortek Aquadopp 600-kHz Z-cell profiler were used. The vertical cell size was 1 m and the sampling interval 600 s or 1200 s. More details about the current meters can be found at https://www.nortekgroup.com/.

We compare modeled and measured currents at the ADCP site during two spring-summer periods (Table 1) covering the important migration periods of wild salmonid fish (see Introduction). The depth range of the observation data used in this study goes from the surface to 15 m depth for the sampling period covering the narrowest depth range and down to 50 m depth for the period covering the largest depth range (Table 1). Current and wind strengths at the ADCP site and other fjord locations, are always presented for vectors directed "along the fjord" which we define as in southwest-northeast direction with northeast (into the fjord) as positive.

2.3. Method for model validation

In this study, we use the accuracy measure index λ suggested by Duveiller et al. (2016):

$$\lambda = 1 - \frac{\sum_{i=1}^{n}(X_i - Y_i)^2}{\sum_{i=1}^{n}\left(X_i - \overline{X}\right)^2 + \sum_{i=1}^{n}\left(Y_i - \overline{Y}\right)^2 + n\left(\overline{X} - \overline{Y}\right)^2 + k}$$

$$= 1 - \frac{n^{-1}\sum_{i=1}^{n}(X_i - Y_i)^2}{\sigma_X^2 + \sigma_Y^2 + \left(\overline{X} - \overline{Y}\right)^2 + k}$$

$$k = \begin{pmatrix} 0, & \text{if } r \geq 0 \\ 2\left|\sum_{i=0}^{n}\left(X_i - \overline{X}\right)\left(Y_i - \overline{Y}\right)\right|, & \text{otherwise} \end{pmatrix}$$

In the equation, X_i = modeled current at timestep i, Y_i = observed current at timestep i, and n = number of timesteps in the comparison period. $\overline{X}$ and $\overline{Y}$ are averaged modeled and observed currents over the comparison period. σ_x and σ_y are standard deviations of modeled and observed currents over the same period. r is the Pearson correlation coefficient. When $r < 0$, then $\lambda = 0$. When $r \geq 0$ and when there is no additive nor multiplicative bias, $\lambda = r$. If there is a bias, the index will take a lower value than r according to a multiplicative coefficient α that can only take a value between 0 and 1:

$$\lambda = \alpha \cdot r = \frac{2}{\sigma_X \Big/ \sigma_Y + \sigma_Y \Big/ \sigma_X + \left(\overline{X} - \overline{Y}\right)^2 \Big/ (\sigma_X \sigma_Y)} \cdot r.$$

λ can be considered as a natural extension to r that downregulates the value of r according to the encountered bias. It is thereby directly interpretable with respect to the Pearson correlation coefficient r.

We choose a critical bias value for λ, denoted λ_{crit}, setting the limits for decent model performance. The model performance is divided into three categories and colored accordingly (Fig. 2): Green color denotes "good" performance, yellow means "medium" and red "poor". For $\lambda \geq \lambda_{crit}$, we categorize the model performance as good and color those time periods green. The closer the λ value is to 1, the better is the correspondence between the model result and the observed along-fjord current speed. For $\lambda < \lambda_{crit}$ we categorize the model performance as either medium or poor, denoted with yellow and red colors, respectively. A poor model state is when there is a net transport in the wrong direction in the model compared with the measurements during the defined

Table 1
Comparison periods presented in this manuscript.

Season	Comparison period (model vs measurements)	Depth range measurements
spring-summer 2016	27.4–27.6	0–45 m
	1.7–16.8	0–40 m
	18.8–30.8	1–50 m
spring-summer 2017	3.5–31.7	0–15 m

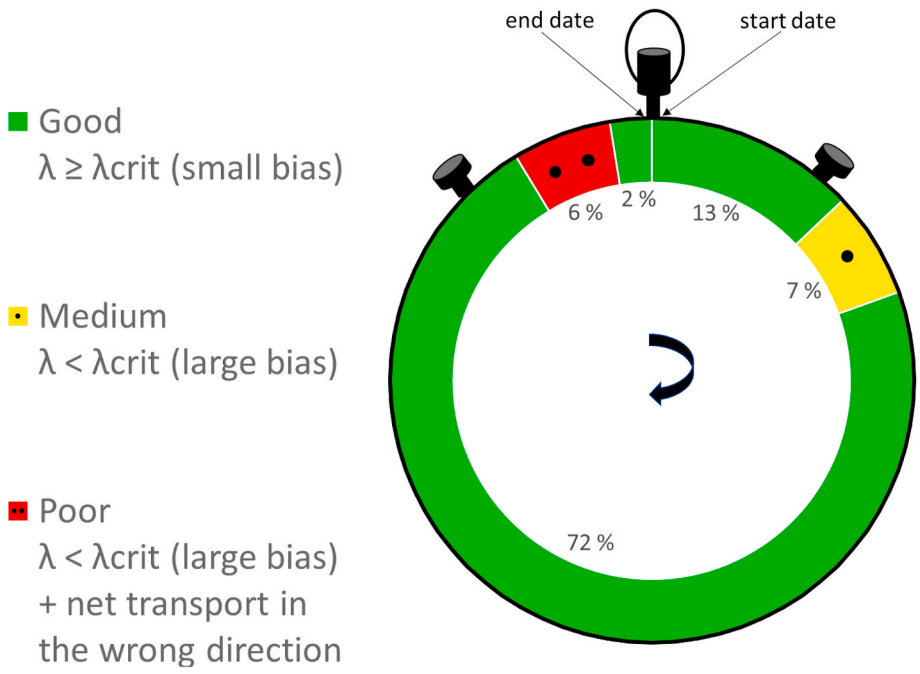

Fig. 2. Schematic showing categorization of model performance (left) and an example on calculation of how much of the time the model falls into the different performance categories over a given time-frame (start date-end date) (right). The example is for the ADCP site in the mid fjord (Fig. 1) and along-fjord current at 0.5 m depth in the spring-summer 2017 (start date = 03.05, end date = 31.07) analyzed in detail in the Results section. The model shows poor performance (red with 2 black dots) 6%, has medium performance (yellow and black dot) 7% and good performance (green) 87% (13 + 72 + 2%) of the time, respectively. (For interpretation of the references to color in this figure legend, the reader is referred to the Web version of this article.)

period (n). Periods with large bias ($\lambda < \lambda_{crit}$) but with the net modeled transport in the same direction as the observed direction is categorized as medium (Fig. 2). Using the method one can calculate how much of the time the model falls into the different performance categories (Fig. 2). λ_{crit} and the length of the comparison period (n) can easily be changed making the method highly flexible. Sensitivity of the performance classification to the choices of these parameters are demonstrated in the Results section.

3. Results

3.1. Hydrography and currents in the mid of the Hardangerfjord

The numerical model results reproduce observations at or near the ADCP site (see locations on map in Fig. 1) relatively well (Figs. 3–5). For the temperature and salinity profiles we see a classical evolution from spring to summer as a relatively thin upper layer becomes warmer from solar heating (Fig. 3) and a brackish upper layer develops (Fig. 4). The observed profiles are illustrated with filled circles, showing a similar vertical structure as the model results. Also, for the location of the mixed layer depth, approximated as the depth with maximum vertical salinity gradient, the agreement between the observed and modeled values is good (Fig. 4).

The along-fjord current component reveals an episodic flow system, with alternating episodes of inflow and outflow (Fig. 5), particularly at intermediate depths. The inflow events tend to be 0.1–0.3 m/s stronger than the outflow events. As noted in the Introduction such patterns typically occur when internal waves of coastal origin propagate into the fjord. Near the surface local wind forcing or brackish layer flow often become more important and the flow is more irregular.

3.2. Demonstration of model validation method in the Hardangerfjord

Though visual inspection of comparable figures (previous section) is useful for assessing a general impression of model performance it can seldom be used to compare models or detect reasons for good or poor model performance. In the following we show how using the new quantitative and index-based model validation method provides us with more information.

We demonstrate the method comparing modeled and observed

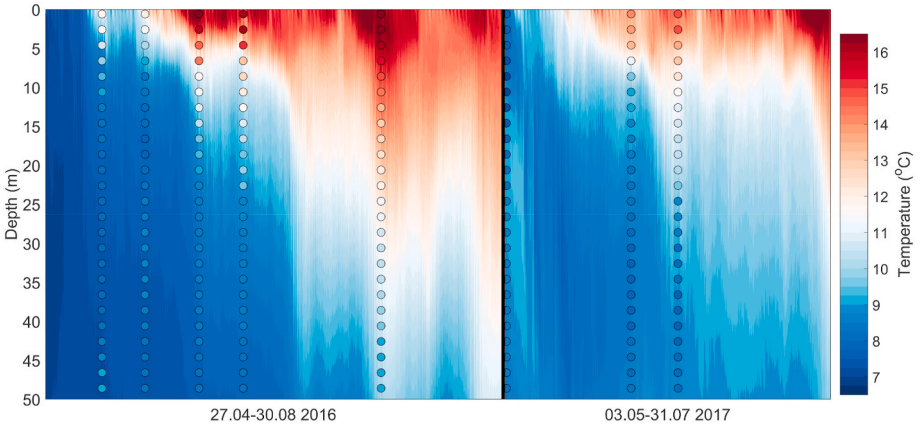

Fig. 3. Temperature in spring-summer 2016 and 2017 in the middle part of the fjord (CTD near ADCP current comparison site, Fig. 1) in model (contours) and measurements (circles).

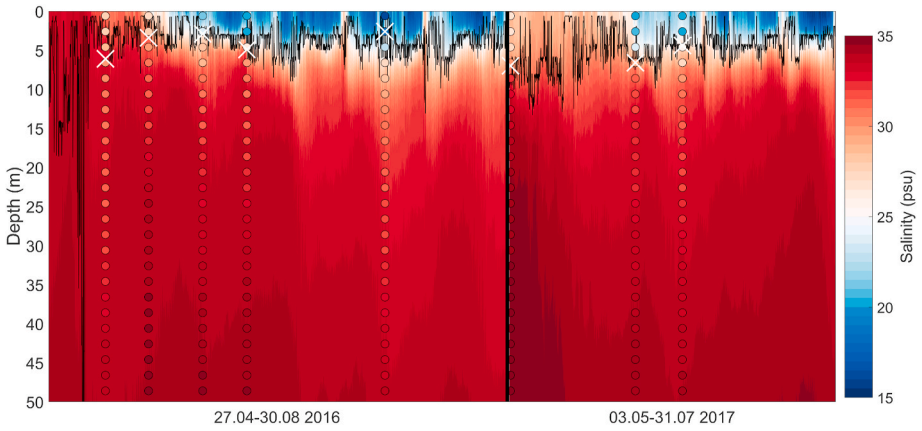

Fig. 4. Salinity in spring-summer 2016 and 2017 in the middle part of the fjord (CTD near ADCP current comparison site) in model (contours) and measurements (circles). Black line and white crosses denote the mixed layer depth in model and measurements, respectively, approximated as the depth with maximum vertical salinity gradient.

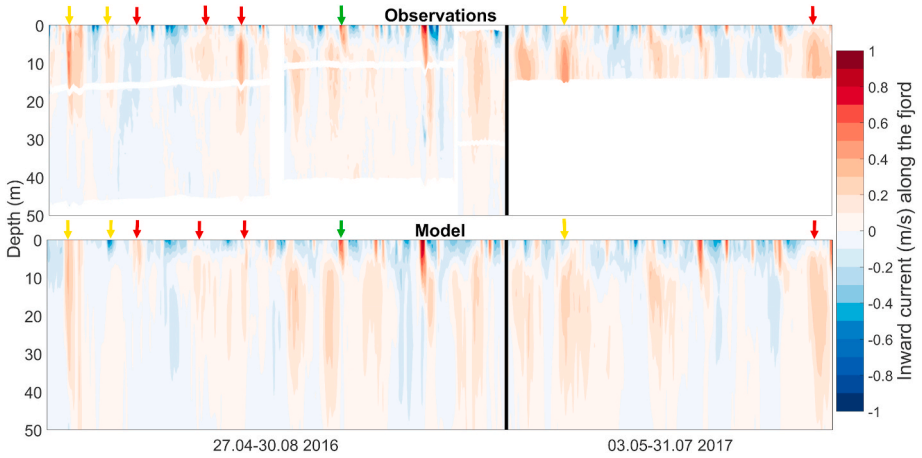

Fig. 5. Current at ADCP site in spring-summer 2016 and 2017, observations and model. Arrows indicate episodes discussed in the coming sections.

along-fjord current speed at 0.5 m depth at the ADCP site (Fig. 6). Since the mixed layer occasionally only is a few meters thick (Fig. 4) we choose this depth level to be sure that the comparison is representative for the mixed layer.

Choices must also be made for λ_{crit} and analysis period (n). A sensitivity study varying n and λ_{crit} is shown in Fig. 7. Varying λ_{crit} in the range 0.02–0.20 would result in almost no changes in the number of occurrences of the different performance categories and quite small changes in their time extension (Figs. 6–7). For $\lambda_{crit} > 0.20$ there will be more periods categorized with medium and poor performance (Fig. 6b) but such values of λ_{crit} will provide a very strict criterion as differences between model and observations then become subtle (Fig. 6a). To have a clear distinction between episodes with good and medium-poor model performance it therefore seems reasonable to choose λ_{crit} in the range 0.02–0.20. Our choice of $\lambda_{crit} = 0.05$ is based on this and similar evaluations at other depths.

A comparison period (n) of 5-days is chosen as biases in modeled currents over such a time frame potentially lead to large misplacement of biological material (e.g. salmon lice) in particle dispersion models. For a typical average model bias of ±0.1 m/s (yellow and red periods) salmon lice may be erroneously misplaced up to 40 km in the model over a 5-day period. Salmon lice originating in the mid-outer fjord where infestation pressure is most problematic (Sandvik et al., 2016a, 2020) could then erroneously be retained in or transported out of the fjord ("escape from the fjord") or go too short or far into the inner fjord. In the inner fjord, salinity levels in the upper water masses are lower and since salmon lice avoid such levels there will also be a large vertical misplacement. Adjusting the comparison period by one day (to 4 or 6 days), keeping λ_{crit} at its preferred level ($\lambda_{crit} = 0.05$), gives small changes in performance (Fig. 7). Performance worsen going down to 2 days (Fig. 7). However, keeping the same λ_{crit} for 2 days and 5 days will result in shorter misplacement of salmon lice over 2 days (quite similar average bias in current speed but it occurs over fewer days). For this study, where distant misplacement (out of the fjord or to the inner fjord) is considered most critical it would probably be reasonable to accept a lower value of λ_{crit} if a period of 2 days was chosen.

3.3. Characteristics for periods with good model performance

The model often performs well in 2016 (green color 64% of the time in Fig. 6) and particularly well in 2017 (87% of the time). During these periods, there is often quite good correlation ($r > 0.8$) with medium to strong local along fjord wind signals (Fig. 8). Since performance is good, the model must have a realistic local wind field which is confirmed from comparison between modeled and measured wind at the closest measurement site (Fig. 9a).

An example of a situation when the numerical model gives a good representation of the near surface current, is from July 16, 2016 (see green arrows in Figs. 5, 6a and 8). At this day, an along-fjord wind into the Hardangerfjord was present forcing the surface water in the same direction (Fig. 10a).

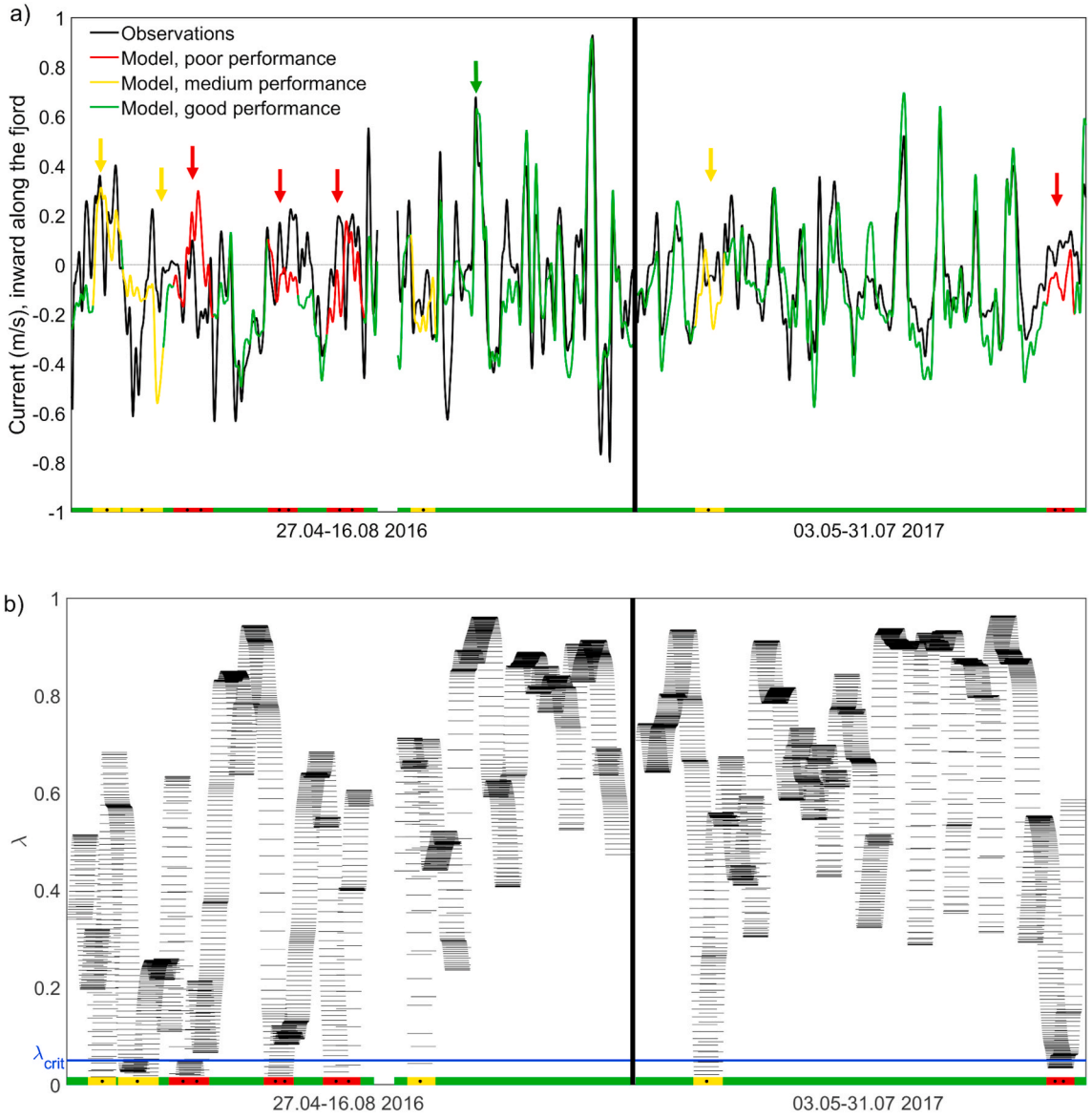

Fig. 6. a) Color categorization of model performance for modeled and observed current at 0.5 m depth at the ADCP site for spring-summer 2016 and 2017 based on λ and λ_{crit}, and net transport direction in model and observations over the same time frame. Arrows show timing of episodes discussed in the coming sections. b) λ at 0.5 m depth in spring-summer 2016 and 2017 over consecutive 5-day periods (black lines). The chosen $\lambda_{crit} = 0.05$ is shown as a blue line. Colors along both the x-axis show model performance. (For interpretation of the references to color in this figure legend, the reader is referred to the Web version of this article.)

3.4. Characteristics for periods with medium and poor model performance

In the first period with medium model performance (1st yellow period in Fig. 6a) strong northward winds on the coastal shelf result in strong coastal currents (Fig. 10b) and on-shore water transport near the surface. This results in downwelling near the fjord mouth which sets up a horizontal pressure gradient strong enough that internal waves propagate all the way into the mid fjord (ADCP site, Fig. 10b). The intrusion of denser coastal water masses near the surface leads to substantial deepening of the fjord mixed layer. During the strongest inflows, the mixed layer lowers to 30–50 m depth (Fig. 4) and temperature, salinity, and currents signals become quite homogenous down to these depths (Figs. 3–5). The measured current is stronger than the modeled near the surface, but the extension of the signal is shallower (1st yellow arrow, Fig. 5).

In the second yellow period (Fig. 6a) the measured current continues to mainly be correlated with the coastal wind signal. Whereas, local fjord wind explains much the model signal (Fig. 8). Coastal signals propagate into the fjord in the model as well (not shown), but not strongly enough to be evident near the surface in the mid fjord (ADCP site).

Most other periods characterized by yellow and red color (arrows, Fig. 6a) can also be explained by remote forced coastal signals not propagating sufficiently far into the fjord in the model to reach the ADCP site. An effect of this is that the signals, typically having broad maximums at intermediate depths, reach closer to the surface in the measurements than in the model during most of these episodes (arrows, Fig. 5).

3.5. Reasons for differences in model performance

At intermediate depths, the inflow episodes with some days' duration (Fig. 5) are typically a result of internal wave propagation from the coast after a period of downwelling. The propagating wave is affected by friction, turbulence and topography on its way, but often these waves reach the ADCP site. The propagation speed is typical for plane internal

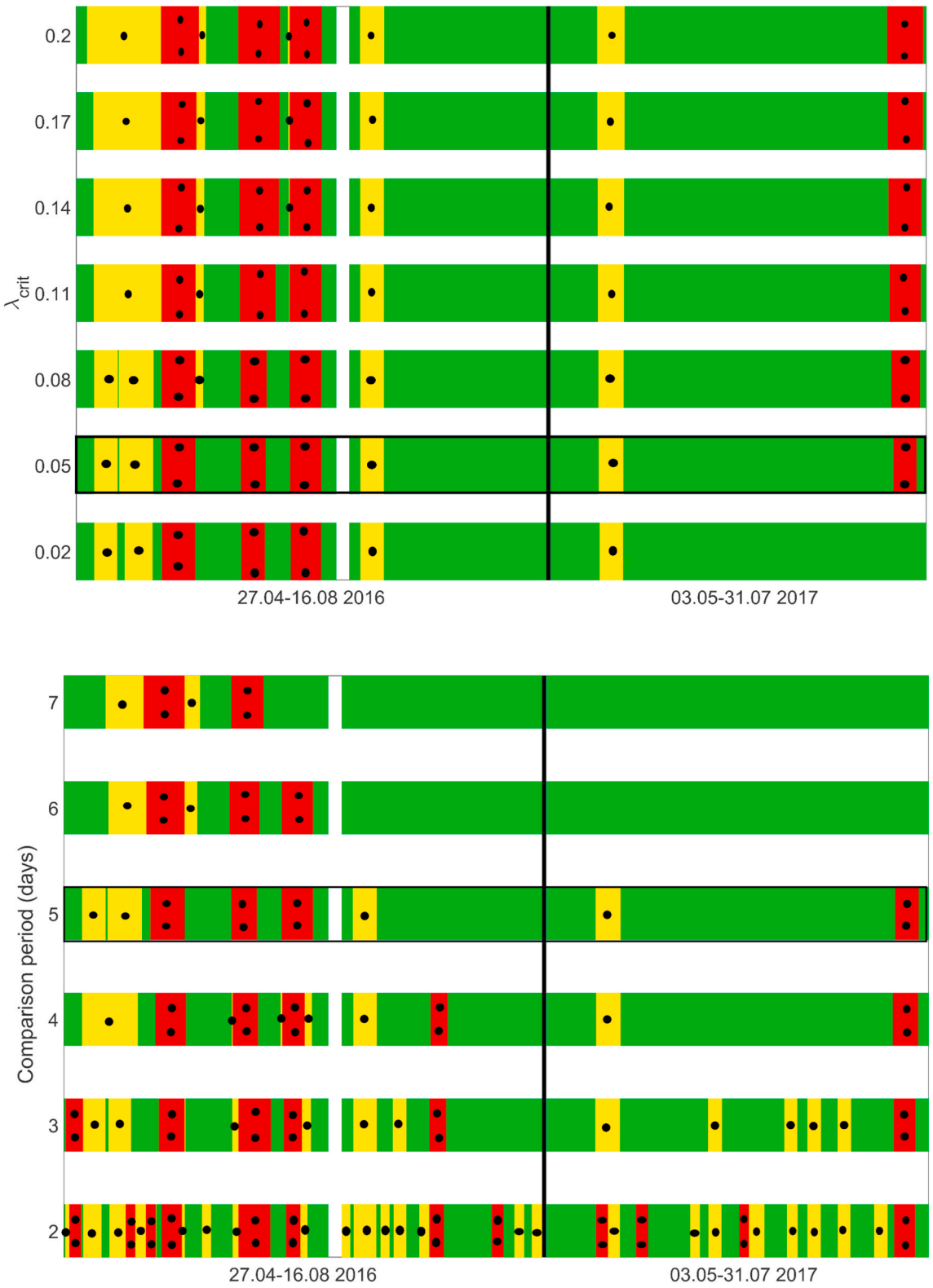

Fig. 7. Color categorization of model performance for current at 0.5 m depth at the ADCP site for different values of λ_{crit} and length of comparison period (n). Upper panel: Varying λ_{crit}, keeping n constant at 5 days. Lower panel: Varying n, with constant $\lambda_{crit} = 0.05$. Performance for our preferred values of λ_{crit} and n is framed by black lines. (For interpretation of the references to color in this figure legend, the reader is referred to the Web version of this article.)

waves and less than 1 m/s (Miropol'sky, 2001).

At 13.5 m depth, close to where we find the strongest intermediate currents (Fig. 5), the modeled along-fjord current is still in relatively good agreement with the observed current (Fig. 11). The green color is occurring 60% of the time and the periods with red color are rather short.

Important for the generation of the internal waves in the fjord mouth region are the direction and strength of the coastal wind and the water

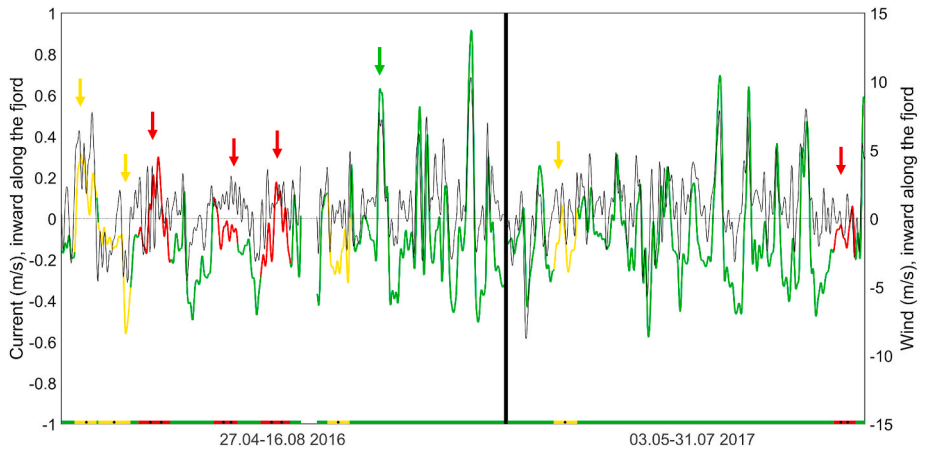

Fig. 8. Modeled current near the surface (0.5 m depth, model performance shown using colors) and modeled along-fjord wind (black line) at the ADCP site (location shown in Fig. 1) during spring-summer 2016 and 2017. The current signals are detided (see Methods) and 24hr lowpass filtered. The wind signals are 24hr lowpass filtered. (For interpretation of the references to color in this figure legend, the reader is referred to the Web version of this article.)

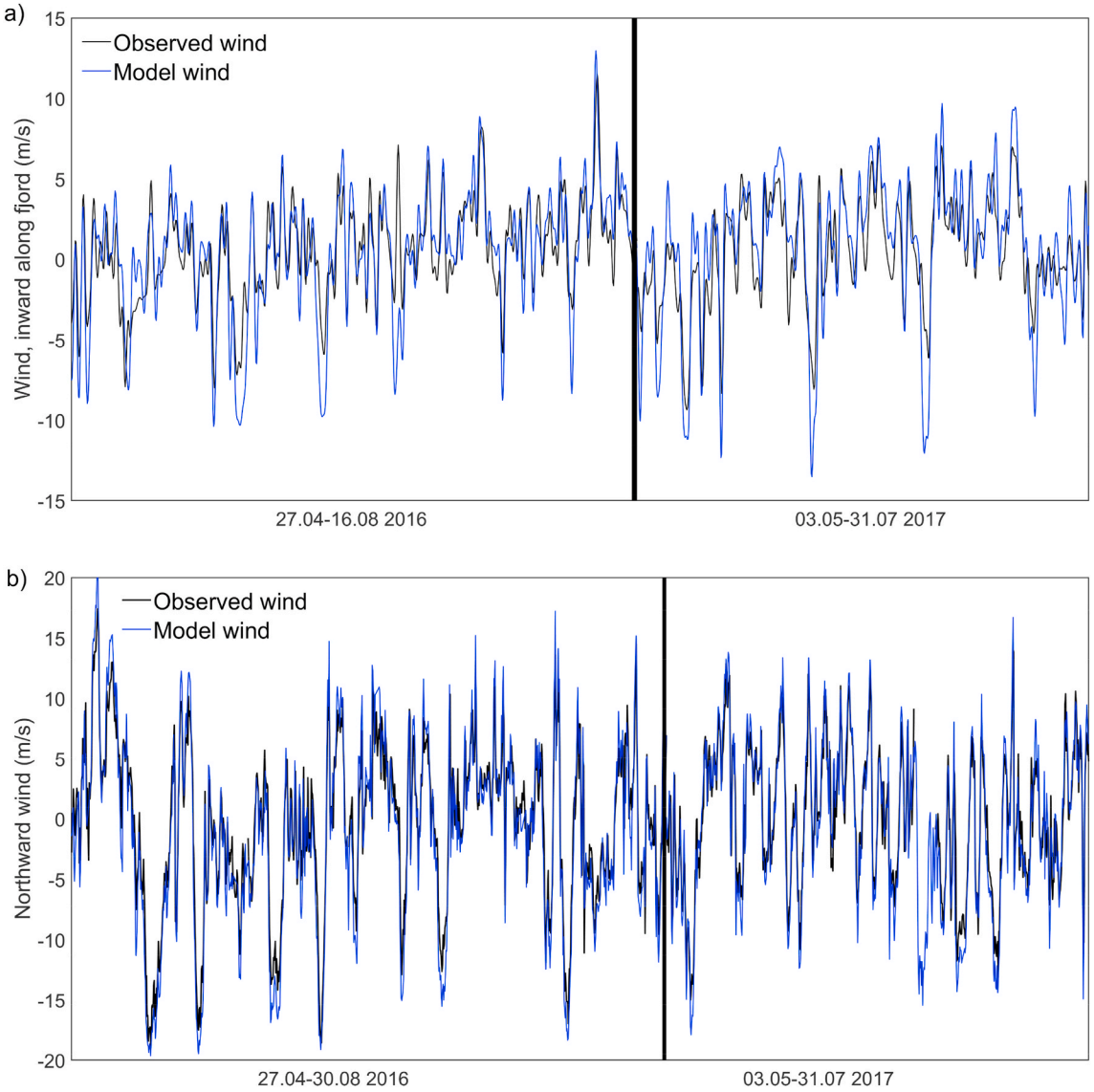

Fig. 9. Comparison of modeled and measured wind components (every 3rd hour) in spring-summer 2016 and 2017 at: a) Kvamsøy and b) Utsira (see locations in Fig. 1).

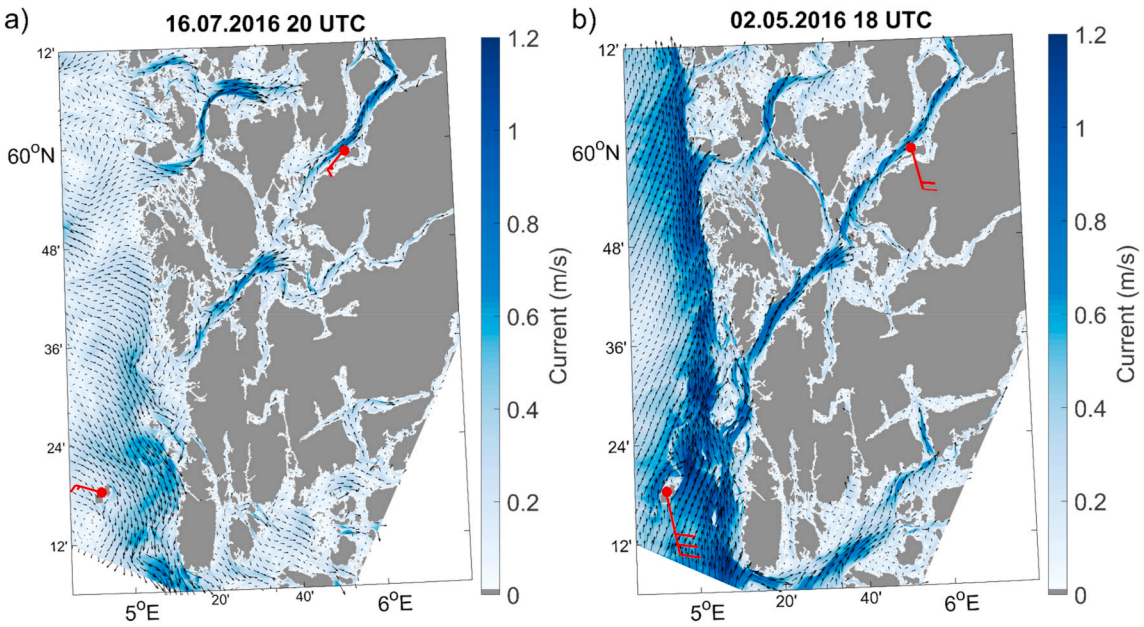

Fig. 10. Near surface model currents (0.5 m depth) in the outer-mid fjord. a) 16.07 2016 20 UTC, green arrows in Figs. 5 and 6a b) 2.5 2016 18 UTC, first yellow arrows in Figs. 5 and 6a, respectively. Black arrows show current direction. The arrow lengths are scaled according to current strength (blue contours). Red wind barbs show wind direction at Utsira and the ADCP site. Wind speed shown on barb tails: One short line for every 1 m/s, one long line for every 5 m/s. The size of the wind barbs is scaled relative to each other based on the wind speed. (For interpretation of the references to color in this figure legend, the reader is referred to the Web version of this article.)

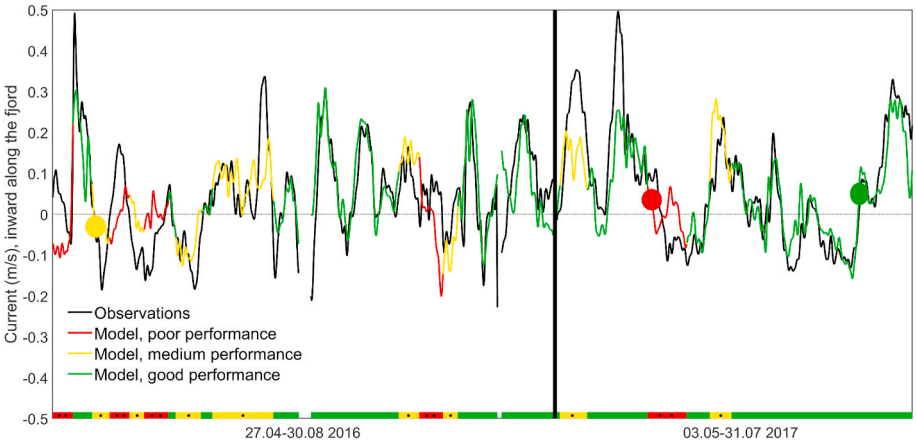

Fig. 11. Model performance at 13.5 m depth at the ADCP site for spring-summer 2016 and 2017. Colored dots show timing of outer Utsira salinity profiles shown in Fig. 12.

mass stratification. The correspondence between modeled and measured coastal wind is very good (Fig. 9b). Periods with medium and poor model performance are therefore not caused by errors in the modeled coastal wind field. As discussed in the methods section we use temperature and salinity profiles at outer Utsira monitoring station as a proxy for the coastal stratification. Comparing profiles of temperature and salinity at this offshore site, we find that the model quality for salinity varies widely. We extract three episodes as examples, a green, yellow and red period, respectively (Fig. 12). We clearly see that the salinity structure in the NorFjords-160 model is too weak for the two episodes with medium (yellow) and poor (red) model performance at the ADCP site and that the model replicates the observed offshore salinity profile in the good (green) period.

The episodes with too weak stratification often occur in spring. Associated up-/downwelling due to a given coastal forcing (e.g. alongshore coastal wind) induces a too small density perturbation near the fjord mouth and thereby a too weak pressure gradient across the coastal shelf. Internal wave propagation into the fjord therefore becomes too weak. In general, the vertical structures of the coastal salinities in the model are more realistic in July–August. The model performance in the mid fjord is then improved both with regards to currents at intermediate depth (Fig. 11) and near the surface (Fig. 6a), along with a more realistic representation of the surface mixed layer depth (Fig. 4).

Outer Utsira is positioned close to the NorFjords-160 open model boundaries. The deviations in the model's stratification may therefore be linked to any biases in the boundary conditions. We find that the salinity and temperature profiles at outer Utsira are quite similar in both Norfjords-160 and NorKyst-800 (Fig. 12), the latter model providing boundary conditions for the finer scale model. The NorFjords-160 performance is therefore likely influenced by biases that already has been generated in the NorKyst-800 model.

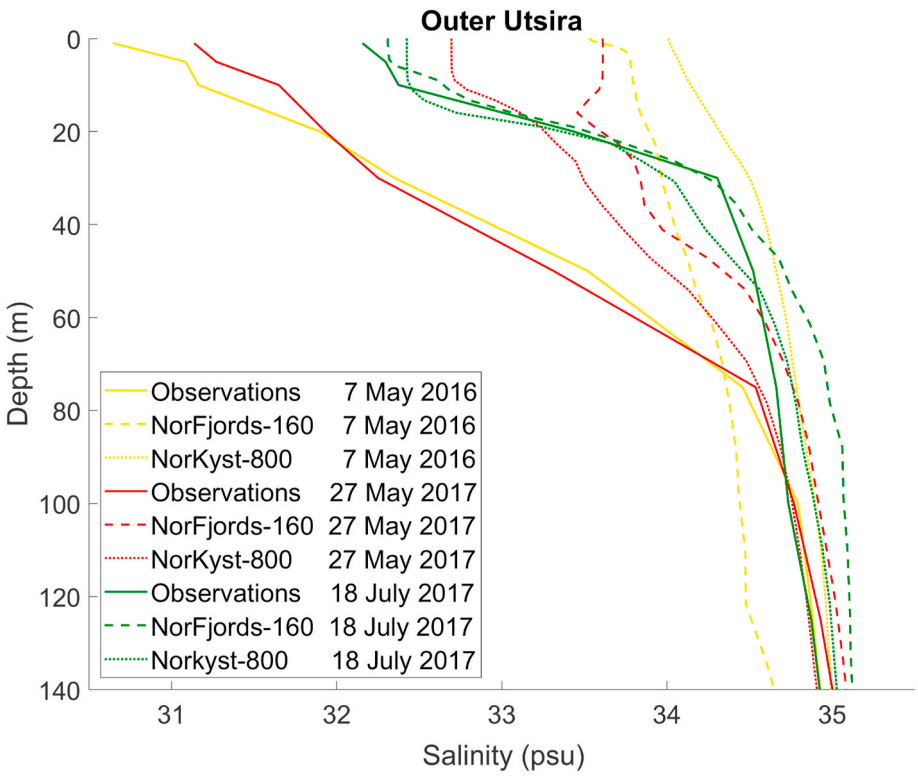

Fig. 12. Salinity at outer Utsira (location shown in Fig. 1) in observations, NorFjords-160 model, and NorKyst-800 model (model providing boundary conditions) in periods (dots Fig. 11) with good (green color), medium (yellow color) and poor (red color) mid-fjord performance at intermediate depths. (For interpretation of the references to color in this figure legend, the reader is referred to the Web version of this article.)

4. Discussion

An advantage with the presented validation method is flexibility (e.g. possibility to vary the comparison period (n) and accuracy index (λ_{crit})) and computational efficiency (easy to perform sensitivity studies). Due to this we suggest applicability for a broad set of geophysical variables and physical environments. The method could for instance have been used if we wanted to make a more detailed evaluation of the observed and modeled wind fields (Fig. 9). λ_{crit} and n should be set independently in each study. Depending on the purpose of the study, assessment should be performed related to what is considered as an acceptable "bias" (λ_{crit}) and the most relevant time-frame (n) for the main applications. A sensitivity study of the type shown in the Results section could be one way to make such an evaluation.

This study shows application for hydrodynamic model performance in the Hardangerfjord. Improving performance through better representation of the physical processes causing model biases in the Hardangerfjord will be the scope of a following up study. We therefore only briefly discuss possible approaches here. One approach could be to test using a larger model domain having the open boundaries further away from the coastal shelf. However, this comes with a cost in the form of enhanced demand on computing time and storage capacity. Biases would probably persist but could be moved to a region further offshore thereby having less influence on the fjord dynamics.

One-way nesting is applied at the open boundaries in NorFjords-160. By implementing two-ways nesting we will allow implication of fjord dynamics from NorFjords-160 not resolved in the coarser coastal model (NorKyst-800). Running both the 800 m-model and the 160 m-model in parallel exchanging state along the open boundaries of the fine scale model may be an approach that potentially could alleviate the problem to some degree.

Data assimilation, combining the numerical model and observations to obtain a better representation of the coastal stratification in the model could be tested if more measurements become available. This demands a coastal observational network with high spatial resolution. Measurements must also occur frequently as our analysis reveals that the performance of the model in its current state varies within the time scale of a few days.

Though coastal stratification biases seem to be important, local factors in the Hardangerfjord may also contribute to model biases. Mixing with side fjords dampen the internal waves propagating into the main fjord and incorrect circulation in side-fjords could have some impact. Inaccurate local turbulent mixing may also be a contributing factor and use of different parametrization schemes for mixed layer turbulence could be tested. Since the river discharge is based on measurements associated with the main rivers, we expect them to be realistic. The measurements do not cover all rivers and there could in some cases be regulations downstream of the measurements in dams used for production of hydropower. Therefore, there are some uncertainties in the downstream fluxes entering the fjord, particularly related to timing of the discharged freshwater. However, river discharge was not identified as a single major cause for the episodes with medium or poor model performance for near surface currents.

The effects of small-scale spatial variability might be important. The internal Rossby radius of deformation will have a length comparable to the fjord width, and uneven topography and coastline affect the currents. Eddies are created in the widest fjord areas, fjord crossings, and bends. A timely question is then whether there is a large chance for spatial model error (i.e. incorrect placement and shape of current features (Sandvik et al., 2016b)) as we in the comparisons with observations at the ADCP site use model values from the closest grid cell to the measurement locations. We tested this by comparing the model currents using the nearest grid cell, the average of the nine closest grid cells, and the grid cells with maximum and minimum values within these nine cells. This showed rather modest model variability near the ADCP site. Using the closest grid cell should therefore not lead to large bias in the

evaluation of model performance at this site.

All the major driving factors for the circulation in the Hardangerfjord (local fjord wind, river discharge, alongshore coastal wind, and stratification in coastal waters) are expected to be strongly altered with future climate change (Hanssen-Bauer et al., 2017). This would affect the balance between external and local forcers and thereby the propagation of internal waves and the coast-fjord exchange. The proportion of the fjord having water masses with a strong coastal signature could thereby change in the future. This could further affect the frequency of water renewal below sill level, a topic not focused upon in this study due to its rather narrow time frame of a few years.

5. Conclusions

This study presents a new method for validation of hydrodynamic fjord models when current observations are available. The method uses an easily computable accuracy measure index and is flexible with regards to performance criteria limits and assessed time frames. Model performance can be presented in an intuitive form. We also demonstrate how further analysis can derive the major forcings decisive for the fjord circulation. Combining this with the validation method makes it possible to find causes for good and poor model performance and whether poor performance is caused by systematic model biases.

We tested the method in the mid of the Hardangerfjord having frequent current measurements and topical biological and environmental issues (salmon lice infestation pressure and other matters outlined in the Introduction). Our applied fjord model performs well most of the time. In the mixed layer, good performance often occurs when currents are correlated with the local wind field, suggesting that the model is driven by realistic input data for local wind. Both in the mixed layer and at intermediate depths, poor performance occurs when internal waves induced by pressure perturbations on the coastal shelf propagate erroneously into the fjord. Coastal stratification errors in the model connected to deviations in the boundary conditions for salinity are likely the major cause.

Though we focused on currents in a Norwegian fjord, we propose that the flexibility of the validation method makes it applicable for model evaluation in any part of the world's ocean. The necessary data is a continuous observational time series and corresponding model results. In addition, this method is also very likely applicable for other variables describing the physical or chemical environment.

Funding

This research is mostly financed by the Institute of Marine Research internal fjord and coastal climate project (internal project no. 14894). Thanks to the crew on the research vessels collecting data.

Credit author statement

Stig B. Dalsøren: Conceptualization, Methodology, Software, Validation, Formal analysis, Investigation, Data Curation, Writing - Original Draft, Writing - Review & Editing, Visualization. **Jon Albretsen:** Conceptualization, Methodology, Software,Validation, Formal analysis, Investigation, Resources, Data Curation, Writing - Original Draft, Writing - Review & Editing, Visualization, Supervision. **Lars Asplin:** Conceptualization, Methodology, Software ,Validation, Formal analysis, Investigation, Resources, Data Curation, Writing - Original Draft, Writing - Review & Editing, Visualization, Supervision, Project administration, Funding acquisition.

Declaration of competing interest

The authors declare that they have no known competing financial interests or personal relationships that could have appeared to influence the work reported in this paper.

Acknowledgements

The simulations were performed on resources provided by UNINETT Sigma 2 - the National Infrastructure for High Performance Computing and Data Storage in Norway.

References

Adams, T.P., Proud, R., Black, K.D., 2015. Connected networks of sea lice populations: dynamics and implications for control. Aquaculture Environment Interactions 6, 273–284.

Albretsen, J., Aure, J., Saetre, R., Danielssen, D., 2011. Climatic variability in the Skagerrak and coastal waters of Norway. ICES (Int. Counc. Explor. Sea) J. Mar. Sci. 69, 758–763. https://doi.org/10.1093/icesjms/fsr187.

Armstrong, J.S., 2001. Evaluating forecasting methods. In: Armstrong, J.S. (Ed.), Principles of Forecasting: A Handbook for Researchers and Practitioners. Kluwer.

Armstrong, J.S., Collopy, F., 1992. Error measures for generalizing about forecasting methods: empirical comparisons. Int. J. Forecast. 8, 69–80. https://doi.org/10.1016/0169-2070(92)90008-W.

Arneborg, L., Erlandsson, C.P., Liljebladh, B., Stigebrandt, A., 2004. The rate of inflow and mixing during deep-water renewal in a sill fjord. Limnol. Oceanogr. 49, 768–777. https://doi.org/10.4319/lo.2004.49.3.0768.

Asplin, L., Albretsen, J., Johnsen, I.A., Sandvik, A.D., 2020. The hydrodynamic foundation for salmon lice dispersion modeling along the Norwegian coast. Ocean Dynam. https://doi.org/10.1007/s10236-020-01378-0.

Asplin, L., Johnsen, I.A., Sandvik, A.D., Albretsen, J., Sundfjord, V., Aure, J., Boxaspen, K.K., 2014. Dispersion of salmon lice in the Hardangerfjord. Mar. Biol. Res. 10, 216–225. https://doi.org/10.1080/17451000.2013.810755.

Asplin, L., Salvanes, A.G.V., Kristoffersen, J.B., 1999. Nonlocal wind-driven fjord–coast advection and its potential effect on plankton and fish recruitment. Fish. Oceanogr. 8, 255–263. https://doi.org/10.1046/j.1365-2419.1999.00109.x.

Azad, A.M., Frantzen, S., Bank, M.S., Johnsen, I.A., Tessier, E., Amouroux, D., Madsen, L., Maage, A., 2019. Spatial distribution of mercury in seawater, sediment, and seafood from the Hardangerfjord ecosystem, Norway. Sci. Total Environ. 667, 622–637. https://doi.org/10.1016/j.scitotenv.2019.02.352.

Castillo, M.I., Pizarro, O., Ramírez, N., Cáceres, M., 2017. Seiche excitation in a highly stratified fjord of southern Chile: the Reloncaví fjord. Ocean Sci. 13, 145–160. https://doi.org/10.5194/os-13-145-2017.

Chapman, D.C., 1985. Numerical treatment of cross-shelf open boundaries in a barotropic coastal ocean model. J. Phys. Oceanogr. 15, 1060–1075. https://doi.org/10.1175/1520-0485(1985)015<1060:Ntocso>2.0.Co;2.

Chen, C., Twycross, J., Garibaldi, J.M., 2017. A new accuracy measure based on bounded relative error for time series forecasting. PloS One 12, e0174202. https://doi.org/10.1371/journal.pone.0174202.

Clements, M.P., Hendry, D.F., 1993. On the limitations of comparing mean square forecast errors. J. Forecast. 12, 617–637. https://doi.org/10.1002/for.3980120802.

Crosbie, T., Wright, D.W., Oppedal, F., Dalvin, S., Myksvoll, M.S., Dempster, T., 2020. Impact of thermoclines on the vertical distribution of salmon lice larvae. Aquaculture Environment Interactions 12, 1–10.

Crosbie, T., Wright, D.W., Oppedal, F., Johnsen, I.A., Samsing, F., Dempster, T., 2019. Effects of step salinity gradients on salmon lice larvae behaviour and dispersal. Aquaculture Environment Interactions 11, 181–190.

Davidsen, J.G., Plantalech Manel-la, N., ØKland, F., Diserud, O.H., Thorstad, E.B., Finstad, B., Sivertsgård, R., McKinley, R.S., Rikardsen, A.H., 2008. Changes in swimming depths of Atlantic salmon Salmo salar post-smolts relative to light intensity. J. Fish. Biol. 73, 1065–1074. https://doi.org/10.1111/j.1095-8649.2008.02004.x.

Duveiller, G., Fasbender, D., Meroni, M., 2016. Revisiting the concept of a symmetric index of agreement for continuous datasets. Sci. Rep. 6, 19401. https://doi.org/10.1038/srep19401.

Egbert, G.D., Erofeeva, S.Y., 2002. Efficient inverse modeling of barotropic ocean tides. J. Atmos. Ocean. Technol. 19, 183–204. https://doi.org/10.1175/1520-0426(2002)019<0183:Eimobo>2.0.Co;2.

Farmer, D.M., Freeland, H.J., 1983. The physical oceanography of Fjords. Prog. Oceanogr. 12, 147–219. https://doi.org/10.1016/0079-6611(83)90004-6.

Filbee-Dexter, K., Pedersen, M.F., Fredriksen, S., Norderhaug, K.M., Rinde, E., Kristiansen, T., Albretsen, J., Wernberg, T., 2020. Carbon export is facilitated by sea urchins transforming kelp detritus. Oecologia 192, 213–225. https://doi.org/10.1007/s00442-019-04571-1.

Fildes, R., 1992. The evaluation of extrapolative forecasting methods. Int. J. Forecast. 8, 81–98. https://doi.org/10.1016/0169-2070(92)90009-X.

Flather, R.A., 1976. A tidal model of the northwest European continental shelf. Mem. Soc. R. Sci. Liege 10, 141–164.

Foreman, M.G.G., Guo, M., Garver, K.A., Stucchi, D., Chandler, P., Wan, D., Morrison, J., Tuele, D., 2015. Modelling infectious hematopoietic necrosis virus dispersion from marine salmon farms in the discovery islands, British columbia, Canada. PloS One 10, e0130951. https://doi.org/10.1371/journal.pone.0130951.

Gillibrand, P.A., Willis, K.J., 2007. Dispersal of sea louse larvae from salmon farms: modelling the influence of environmental conditions and larval behaviour. Aquat. Biol. 1, 63–75.

Grefsrud, E.S., Svåsand, T., Glover, K., Husa, V., Hansen, P.K., Samuelsen, O., Sandlund, N., Stien, L.H., 2019. Risikorapport norsk fiskeoppdrett 2019 (Risk assessment of Norwegian fin fish aquaculture 2019). In: Grefsrud, E.S., Svåsand, T.,

Glover, K., Husa, V., Hansen, P.K., Samuelsen, O., Sandlund, N., Stien, L.H. (Eds.), Fisken Og Havet. Institute for Marine Research, p. 115.
Haidvogel, D.B., Arango, H., Budgell, W.P., Cornuelle, B.D., Curchitser, E., Di Lorenzo, E., Fennel, K., Geyer, W.R., Hermann, A.J., Lanerolle, L., Levin, J., McWilliams, J.C., Miller, A.J., Moore, A.M., Powell, T.M., Shchepetkin, A.F., Sherwood, C.R., Signell, R.P., Warner, J.C., Wilkin, J., 2008. Ocean forecasting in terrain-following coordinates: formulation and skill assessment of the Regional Ocean modeling system. J. Comput. Phys. 227, 3595–3624. https://doi.org/10.1016/j.jcp.2007.06.016.
Hanssen-Bauer, I., Førland, E.J., Haddeland, I., Hisdal, H., Mayer, S., Nesje, A., Nilsen, J. E.Ø., Sandven, S., Sandø, A.B., Sorteberg, A., Ådlandsvi, B., 2017. Climate in Norway 2100. NCCS report, Miljødirektoratet, p. 47.
Husa, V., Kutti, T., Ervik, A., Sjøtun, K., Hansen, P., Aure, J., 2014. Regional impact from fin-fish farming in an intensive production area (Hardangerfjord, Norway). Mar. Biol. Res. 10, 241–252. https://doi.org/10.1080/17451000.2013.810754.
Inall, M.E., Gillibrand, P.A., 2010. The physics of mid-latitude fjords: a review. Geological Society, London, Special Publications 344, 17–33. https://doi.org/10.1144/sp344.3.
Inall, M.E., Nilsen, F., Cottier, F.R., Daae, R., 2015. Shelf/fjord exchange driven by coastal-trapped waves in the Arctic. J. Geophys. Res.: Oceans 120, 8283–8303. https://doi.org/10.1002/2015jc011277.
Jackson, R.H., Lentz, S.J., Straneo, F., 2018. The dynamics of shelf forcing in Greenlandic fjords. J. Phys. Oceanogr. 48, 2799–2827. https://doi.org/10.1175/jpo-d-18-0057.1.
Johnsen, I., Fiksen, Ø., Sandvik, A., Asplin, L., 2014. Vertical salmon lice behaviour as a response to environmental conditions and its influence on regional dispersion in a fjord system. Aquaculture Environment Interactions 5, 127–141. https://doi.org/10.3354/aei00098.
Johnsen, I.A., Asplin, L.C., Sandvik, A.D., Serra-Llinares, R.M., 2016. Salmon lice dispersion in a northern Norwegian fjord system and the impact of vertical movements. Aquaculture Environment Interactions 8, 99–116.
Klinck, J., Obrien, J., Svendsen, H., 1981. A simple model of fjord and coastal circulation interaction. J. Phys. Oceanogr. 11, 1612–1626. https://doi.org/10.1175/1520-0485(1981)011<1612:ASMOFA>2.0.CO;2.
Kragesteen, T., Simonsen, K., Visser, A., Andersen, K., 2018. Identifying salmon lice transmission characteristics between Faroese salmon farms. Aquaculture Environment Interactions 10, 49. https://doi.org/10.3354/aei00252.
Marchesiello, P., McWilliams, J.C., Shchepetkin, A., 2001. Open boundary conditions for long-term integration of regional oceanic models. Ocean Model. 3, 1–20. https://doi.org/10.1016/S1463-5003(00)00013-5.
Mayer, S., Livik, G., Pontoppidan, M., Båserud, L., Løvset, T., 2020. Analyse Av Klimautvikling I Kyst- Og Innlandsregionen I Rogaland –temperature, Nedbør Og Vind – Anbefalinger Om Veien Videre. NORCE Norwegian Research Centre, p. 47.
Miropol'sky, Y.Z., 2001. Dynamics of Internal Gravity Waves in the Ocean, 1 ed. Springer, Dordrecht.
Myksvoll, M.S., Sandvik, A.D., Albretsen, J., Asplin, L., Johnsen, I.A., Karlsen, Ø., Kristensen, N.M., Melsom, A., Skardhamar, J., Ådlandsvik, B., 2018. Evaluation of a national operational salmon lice monitoring system—from physics to fish. PloS One 13, e0201338. https://doi.org/10.1371/journal.pone.0201338.
Müller, M., Homleid, M., Ivarsson, K.-I., Køltzow, M.A.Ø., Lindskog, M., Midtbø, K.H., Andrae, U., Aspelien, T., Berggren, L., Bjørge, D., Dahlgren, P., Kristiansen, J., Randriamampianina, R., Ridal, M., Vignes, O., 2017. AROME-MetCoOp: a nordic convective-scale operational weather prediction model. Weather Forecast. 32, 609–627. https://doi.org/10.1175/waf-d-16-0099.1.
Oyinlola, M.A., Reygondeau, G., Wabnitz, C.C.C., Troell, M., Cheung, W.W.L., 2018. Global estimation of areas with suitable environmental conditions for mariculture species. PloS One 13, e0191086. https://doi.org/10.1371/journal.pone.0191086.
Pawlowicz, R., Beardsley, B., Lentz, S., 2002. Classical tidal harmonic analysis including error estimates in MATLAB using T_TIDE. Comput. Geosci. 28, 929–937. https://doi.org/10.1016/S0098-3004(02)00013-4.
Rogers, L.A., Peacock, S.J., McKenzie, P., DeDominicis, S., Jones, S.R.M., Chandler, P., Foreman, M.G.G., Revie, C.W., Krkošek, M., 2013. Modeling parasite dynamics on farmed salmon for precautionary conservation management of wild salmon. PloS One 8, e60096. https://doi.org/10.1371/journal.pone.0060096.
Salama, N., Rabe, B., 2013. Developing models for investigating the environmental transmission of disease causing agents within open-cage salmon aquaculture. Aquaculture Environment Interactions 4, 91–115. https://doi.org/10.3354/aei00077.
Salama, N.K.G., Dale, A.C., Ivanov, V.V., Cook, P.F., Pert, C.C., Collins, C.M., Rabe, B., 2018. Using biological–physical modelling for informing sea lice dispersal in Loch Linnhe, Scotland. J. Fish. Dis. 41, 901–919. https://doi.org/10.1111/jfd.12693.
Samsing, F., Oppedal, F., Dalvin, S., Johnsen, I., Vågseth, T., Dempster, T., 2016. Salmon lice (Lepeophtheirus salmonis) development times, body size, and reproductive outputs follow universal models of temperature dependence. Can. J. Fish. Aquat. Sci. 73, 1841–1851. https://doi.org/10.1139/cjfas-2016-0050.
Sandvik, A.D., Bjørn, P.A., Ådlandsvik, B., Asplin, L., Skarðhamar, J., Johnsen, I.A., Myksvoll, M., Skogen, M.D., 2016a. Toward a model-based prediction system for salmon lice infestation pressure. Aquaculture Environment Interactions 8, 527–542.
Sandvik, A.D., Johnsen, I.A., Myksvoll, M.S., Sævik, P.N., Skogen, M.D., 2020. Prediction of the salmon lice infestation pressure in a Norwegian fjord. ICES (Int. Counc. Explor. Sea) J. Mar. Sci. https://doi.org/10.1093/icesjms/fsz256.
Sandvik, A.D., Skagseth, Ø., Skogen, M.D., 2016b. Model validation: issues regarding comparisons of point measurements and high-resolution modeling results. Ocean Model. 106, 68–73. https://doi.org/10.1016/j.ocemod.2016.09.007.
Shchepetkin, A.F., McWilliams, J.C., 2005. The regional oceanic modeling system (ROMS): a split-explicit, free-surface, topography-following-coordinate oceanic model. Ocean Model. 9, 347–404. https://doi.org/10.1016/j.ocemod.2004.08.002.
Shcherbakov, M., Brebels, A., Shcherbakova, N.L., Tyukov, A., Janovsky, T.A., Kamaev, V.A., 2013. A survey of forecast error measures. World Appl. Sci. J. 24, 171–176. https://doi.org/10.5829/idosi.wasj.2013.24.itmies.80032.
Simonsen, M., Lind, O.C., Saetra, Ø., Isachsen, P.E., Teien, H.-C., Albretsen, J., Salbu, B., 2019. Coastal transport of river-discharged radionuclides: impact of speciation and transformation processes in numerical model simulations. Sci. Total Environ. 669, 856–871. https://doi.org/10.1016/j.scitotenv.2019.01.434.
Sjøtun, K., Husa, V., Asplin, L., Sandvik, A.D., 2015. Climatic and environmental factors influencing occurrence and distribution of macroalgae - a fjord gradient revisited. Mar. Ecol. Prog. Ser. 532, 73–88.
Skarðhamar, J., Albretsen, J., Sandvik, A.D., Lien, V.S., Myksvoll, M.S., Johnsen, I.A., Asplin, L., Ådlandsvik, B., Halttunen, E., Bjørn, P.A., 2018. Modelled salmon lice dispersion and infestation patterns in a sub-arctic fjord. ICES (Int. Counc. Explor. Sea) J. Mar. Sci. 75, 1733–1747. https://doi.org/10.1093/icesjms/fsy035.
Skogen, M., Eknes, M., Asplin, L., Sandvik, A., 2009. Modelling the environmental effects of fish farming in a Norwegian fjord. Aquaculture 298, 70–75. https://doi.org/10.1016/j.aquaculture.2009.10.018.
Stigebrandt, A., 1990. On the response of the horizontal mean vertical density distribution in a fjord to low-frequency density fluctuations in the coastal water. Tellus 42, 605–614. https://doi.org/10.1034/j.1600-0870.1990.t01-1-00010.x.
Stigebrandt, A., 2012. Hydrodynamics and circulation of fjords. In: Bengtsson, L., Herschy, R.W., Fairbridge, R.W. (Eds.), Encyclopedia of Lakes and Reservoirs. Springer Netherlands, Dordrecht, pp. 327–344.
Sundfjord, V., 2010. Volume Transport Due to Coastal Wind-Driven Internal Pulses in the Hardangerfjord. Department of Geosciences. University of Oslo, p. 62.
Svendsen, H., Thompson, R.O.R.Y., 1978. In: Nihoul, J.C.J. (Ed.), Wind-driven circulation in a fjord. Elsevier Oceanography Series. Elsevier, p. 439.
Sætre, R., 2007. The Norwegian Coastal Current: Oceanography and Climate. Tapir Academic Press, Trondheim.
Taranger, G.L., Karlsen, Ø., Bannister, R.J., Glover, K.A., Husa, V., Karlsbakk, E., Kvamme, B.O., Boxaspen, K.K., Bjørn, P.A., Finstad, B., Madhun, A.S., Morton, H.C., Svåsand, T., 2014. Risk assessment of the environmental impact of Norwegian Atlantic salmon farming. ICES (Int. Counc. Explor. Sea) J. Mar. Sci. 72, 997–1021. https://doi.org/10.1093/icesjms/fsu132.
Torrissen, O., Jones, S., Asche, F., Guttormsen, A., Skilbrei, O.T., Nilsen, F., Horsberg, T. E., Jackson, D., 2013. Salmon lice – impact on wild salmonids and salmon aquaculture. J. Fish. Dis. 36, 171–194. https://doi.org/10.1111/jfd.12061.
Wan, D., Hannah, C.G., Foreman, M.G.G., Dosso, S., 2017. Subtidal circulation in a deep-silled fjord: douglas channel, British columbia. J. Geophys. Res.: Oceans 122, 4163–4182. https://doi.org/10.1002/2016jc012022.